

# Effect of Strain on Interactions of $\Sigma 3\{111\}$ Silicon Grain Boundary with Oxygen Impurities from First Principles

Rita Maji, Julia Contreras-García, Eleonora Luppi,\* and Elena Degoli\*

The interaction of grain boundaries (GBs) with inherent defects and/or impurity elements in multicrystalline silicon plays a decisive role in their electrical behavior. Strain, depending on the types of GBs and defects, plays an important role in these systems. Herein, the correlation between the structural and electronic properties of  $\Sigma 3\{111\}$  Si-GB in the presence of interstitial oxygen impurities is studied from the first-principles framework, considering the global and local model of strain. It is observed that the distribution of strain along with the number of impurity atoms modifies the energetics of the material. However, the electronic properties of the considered Si-GBs are not particularly affected by the strain and by the oxygen impurities, unless a very high local distortion induces additional structural defects.

research aims to improve photovoltaic efficiency.<sup>[4]</sup> These improvements are primarily dominated by the electrical properties of mc-Si systems, which remain limited by several types of defects, particularly the interaction between Si grain boundaries (Si-GBs) and intrinsic point defects or impurity atoms, such as oxygen, carbon, nitrogen, etc.<sup>[5]</sup> and many transition metals.<sup>[6–8]</sup> Furthermore, some Si-GBs present residual strain, as detected by an infrared polariscope or Raman spectroscopy,<sup>[9,10]</sup> and relation of strain with longer carrier lifetime<sup>[11]</sup> has been reported. Moreover, the distribution of intrinsic strain and its relation to electrical activity

on as-grown mc-Si have been probed experimentally in recent times as well.<sup>[12–14]</sup> Particularly, for metal precipitates correlation between carrier lifetime, stress and precipitate size has been observed.<sup>[15]</sup> Stress not only leads to fracture and breakage during handling and processing but, through the strain produced, may also influence electrical activity and hence affect the performance of furnished solar cells.<sup>[11,16]</sup> Therefore, strain plays a major role, and whether beneficial or not depends on Si-GB types.

As an intrinsic impurity, a large concentration of oxygen is inherent in mc-Si.<sup>[17]</sup> Oxygen atoms prefer to precipitate at GBs; hence, segregation of oxygen atoms can release the stress, thus lowering the strain energy of the GB.<sup>[18,19]</sup> However, the mechanisms that control the O segregation are not yet fully understood, due to the diverse and complex nature of different GBs. A simple way to deal with this difficulty is to characterize the local structure at each site around the GBs and then observe the connection between the boundary and these local structures to understand how they correlate.

In this work, we use this strategy and we investigate, from first principles, the energetics and the electronic properties of Si-GB  $\Sigma 3\{111\}$  with multiple interstitial oxygen atoms both with and without strain. We consider both tensile and compressive strain. For each configuration and type of strain, we analyze the systems revealing factors that mainly influence the system properties. We compare and discuss different strain varieties that can cause oxygen atoms to interact differently with GBs. Actually, understanding how to characterize the structural properties of GBs and their correlation with the electrical activity can be fundamental to understand and control the properties of a device.

## 1. Introduction

Multicrystalline silicon (mc-Si) is the most widely used elemental material on photovoltaic technology in recent times.<sup>[1–3]</sup> Despite the improvement of various aspects, from purification to cell manufacturing, including the silicon fabrication processes, current


R. Maji  
Dipartimento di Scienze e Metodi dell'Ingegneria  
Università di Modena e Reggio Emilia  
Via Amendola 2 Padiglione Tamburini, I-42122 Reggio Emilia, Italy

J. Contreras-García, E. Luppi  
Laboratoire de Chimie Théorique  
Sorbonne Université and CNRS  
F-75005 Paris, France  
E-mail: eleonora.luppi@sorbonne-universite.fr

E. Degoli  
Dipartimento di Scienze e Metodi dell'Ingegneria  
Università di Modena e Reggio Emilia  
Via Amendola 2 Padiglione Morselli, I-42122 Reggio Emilia, Italy  
E-mail: elena.degoli@unimore.it

E. Degoli  
Centro Interdipartimentale En & Tech  
Tecnopolo di Reggio Emilia  
I-42124 Reggio Emilia, Italy

E. Degoli  
Centro S3  
Istituto Nanoscienze-Consiglio Nazionale delle Ricerche (CNR-NANO)  
Via Campi 213/A, 41125 Modena, Italy

 The ORCID identification number(s) for the author(s) of this article can be found under <https://doi.org/10.1002/pssb.202100377>.

© 2021 The Authors. physica status solidi (b) basic solid state physics published by Wiley-VCH GmbH. This is an open access article under the terms of the Creative Commons Attribution License, which permits use, distribution and reproduction in any medium, provided the original work is properly cited.

DOI: 10.1002/pssb.202100377

## 2. Methodology and GB Structure

Our model of the  $\Sigma 3\{111\}$  Si-GB consists of two grains of Si forming an interface along the crystallographic plane  $\{111\}$  (coincidence site lattice). The two Si grains are misoriented with

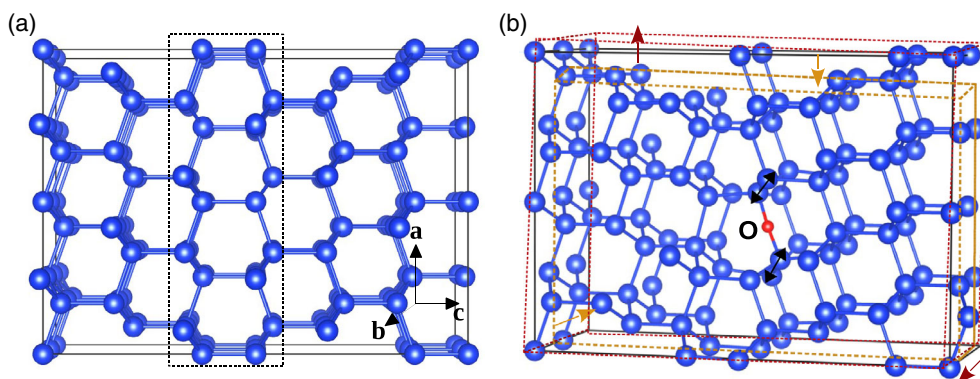


**Figure 1.** a)  $\Sigma 3\{111\}$  Si-GB super-cell: a, b and c are the lattice parameters. The dotted line shows the GB region, b) schematic representation of GS: the cell in black-solid line is the unstrained one, while red dotted line and orange dotted line represents the elongated and compressed cells respectively. LS is also shown through black arrow in some particular bonds neighboring to the O.

respect to one another by an angle  $\Omega = 60^\circ$ . In **Figure 1a**, we show the  $\Sigma 3\{111\}$  orthorhombic supercell ( $a \neq b \neq c$  and  $\alpha = \beta = \gamma = 90^\circ$ ) composed of 96 Si atoms. The lattice parameters are  $a = 13.30 \text{ \AA}$ ,  $b = 7.68 \text{ \AA}$ , and  $c = 18.81 \text{ \AA}$ . A bicystal<sup>[7]</sup> supercell is adopted to follow periodic boundary conditions. A very regular structure of the  $\Sigma 3\{111\}$  Si-GB, that is bond lengths and angles, is close to the Si bulk, which leads to low formation energy.<sup>[19]</sup> Concerning O atoms inclusion in the cell, we have tested many possible inequivalent positions of impurities, as discussed in the study by Rita Maji et al.<sup>[19]</sup> In this article, we focus only on the lowest energy (LE) structures.

The calculations were performed using density functional theory (DFT), as implemented in the plane-wave-based Vienna Ab-initio Simulation Package (VASP).<sup>[20,21]</sup> We employed the generalized gradient approximation of Perdew–Burke–Ernzerhof (PBE) for the exchange-correlation functional and projector

augmented wave (PAW) pseudopotentials with a cutoff of 400 eV. K-point sampling within the Monkhorst–Pack scheme<sup>[22]</sup> was used for integration of Brillouin zone together with the linear tetrahedron method including Blöchl corrections.<sup>[23]</sup> In particular, we used a k-mesh of  $3 \times 3 \times 3$  to calculate energy properties of the structures and a k-mesh of  $7 \times 7 \times 7$  to calculate their density of states (DOS). For the structural optimization, we used as the threshold on the forces the value of  $10^{-2} \text{ eV \AA}^{-1}$  per atom. All post-processing analyses were carried out using the utilities of VESTA.<sup>[24]</sup>

### 3. Results and Discussion

As a first step, in the pristine  $\Sigma 3\{111\}$  Si-GB, we inserted one by one the O atoms considering different initial configurations and optimizing each structure. Starting from the LE configuration

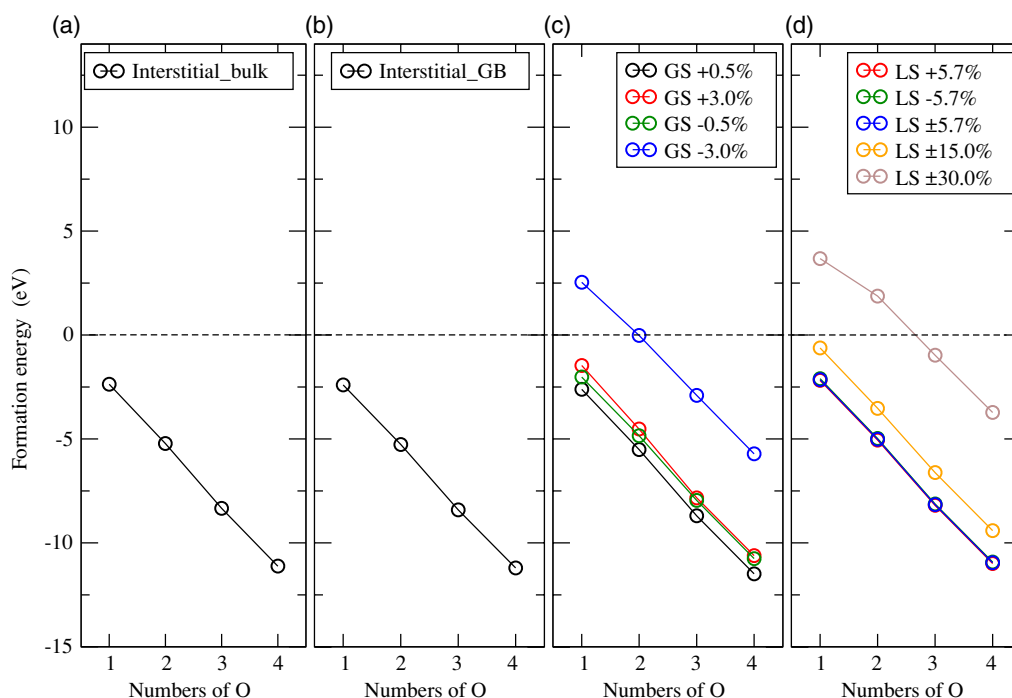


**Figure 2.** Formation energy of interstitial O atoms in a) Si bulk, b)  $\Sigma 3\{111\}$  Si-GB, c) in the presence of GS, and d) LS as mentioned in legends.

with 1O, different possible positions for the second O atoms have been generated and optimized, finally considering the LE configuration with two interstitial O. For three and four oxygen, the same approach has been followed. For each LE configuration structure with 1O, 2O, 3O, and 4O, we calculated the formation energy of oxygen atoms. Moreover, to compare all the Si-GBs structures, we considered O interstitial in Si bulk as a reference. In this case, we used a cubic supercell ( $a = b = c$  and  $\alpha = \beta = \gamma = 90^\circ$ ) of 64 atoms with  $a = 10.86 \text{ \AA}$ .

We always obtain the O atoms at the bond-centered position between two Si atoms and, in the optimized structures, all Si atoms preserve their tetrahedral coordination.<sup>[18,19]</sup> Moreover, the interstitial O atoms can change the structural parameters such as bond lengths and angles, but total energies differ only about 0.01% irrespective of different positions around the GB region.

Considering that, according to literatures,<sup>[8,18,25]</sup> local distortion plays an important role in the segregation mechanism of O atoms, we have modeled the effect of strain on our structures. Starting from the LE  $\Sigma 3\{111\}$  Si-GBs along with different numbers of interstitial O atoms ( $n = 1, 2, 3, \text{ and } 4$ ), the strain was

applied in two different ways, global strain (GS) and local strain (LS), as described in the following paragraphs.

1) GS: in this model, we updated the lattice parameters of the LE O interstitial structure in the  $x$ - and  $y$ -directions, leaving the  $z$ -direction fixed. A schematic example of applied GS is shown in Figure 1b, where an elongation (outward red arrow) and a compression (inward orange arrow) are marked to the  $a$  and  $b$  lattice parameters. These structures are labeled, respectively, GS  $+l\%$  and GS  $-l\%$  for tensile and compressive strain, where  $l$  corresponds to the amount of change with respect to the unstrained lattice parameters of LE configuration. As the elongation or compression is rigidly applied to the whole structure, corresponding changes (elongation or compression) of all bonds in the system are of about the same amount.

2) LS<sup>[19,26]</sup>: in this model, we modified some bond lengths in the interstitial LE structure, creating locally tensile and/or compressive strain in the neighboring Si–Si bonds of O atom(s). In Figure 1b, we show schematically by black arrows that it is a local change and details will be provided in next sections. Elongation/compression or both are labeled as LS  $+p\%$ , LS

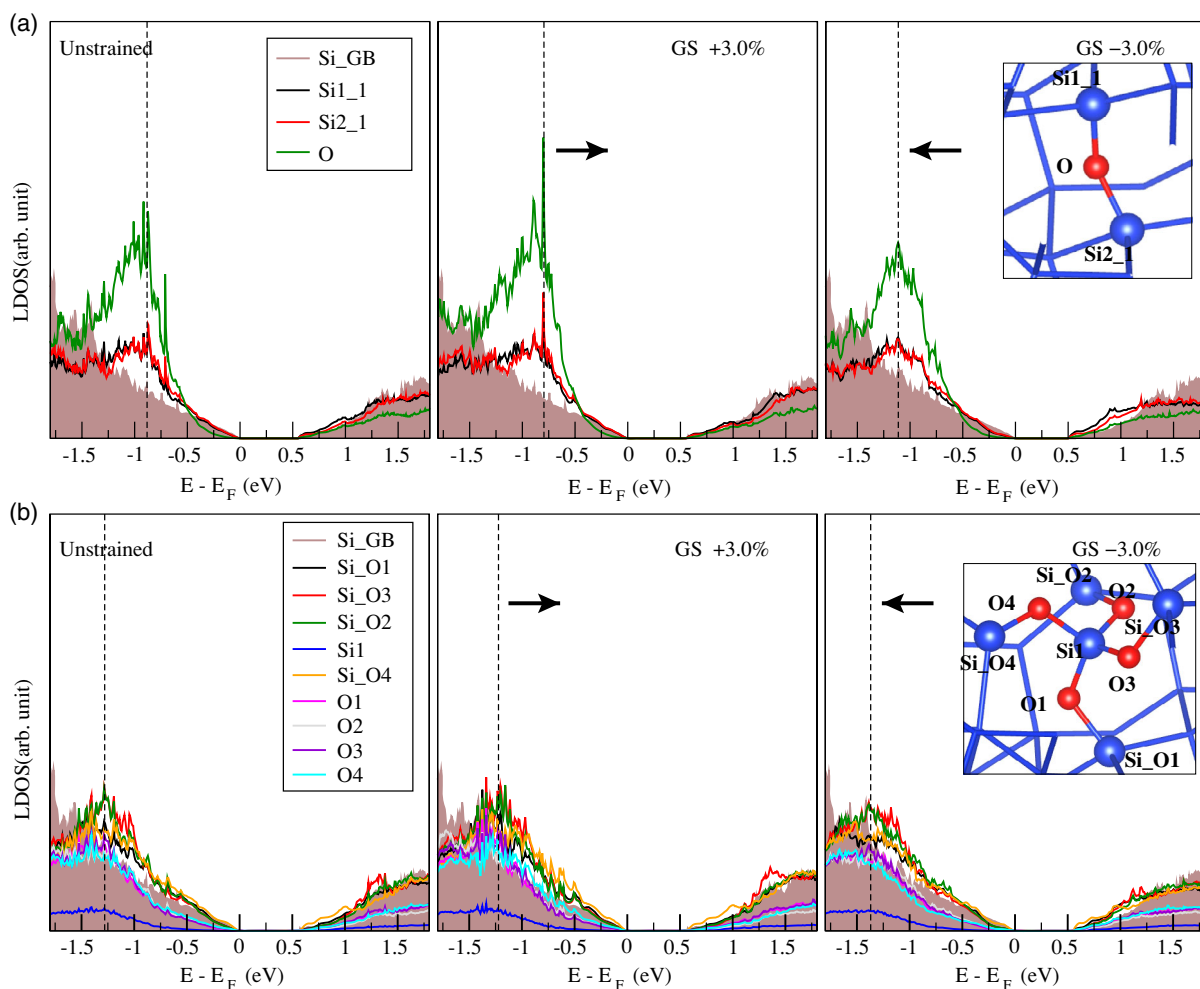


**Figure 3.** LDOS in unstrained, under elongation (GS + 3.0%), and compression (GS – 3.0%) for a) one O atom and two Si atoms bonded with O (inset). b) Four O and all Si atoms connected to O1, O2, O3, and O4 (inset). Si\_GB refers to a Si atom far from the GB region of the pristine GB cell.

$-p\%$ , and LS  $\pm p\%$ , respectively, where  $p$  corresponds to the amount of change with respect to the unstrained bond length of the LE configuration. In the case of LS  $\pm p\%$ , tensile and compressive strain are applied on two different bonds.

To investigate the interaction between the O atoms and the  $\Sigma 3\{111\}$  Si-GB, we calculated the impurity formation energy as

$$E_{\text{Imp}}^{\text{OGB}} = E_{n_{\text{OGB}}} - E_{\text{GB}} - n_{\text{O}}\mu_{\text{O}} \quad (1)$$

where  $E_{n_{\text{OGB}}}$  and  $E_{\text{GB}}$  are the total energies of the GB, including  $n_{\text{O}}$  number of O atoms and of the pristine GB, respectively.  $\mu_{\text{O}}$  is the chemical potential of oxygen calculated as the energy per atom of an  $\text{O}_2$  molecule in vacuum.

This quantity has to be compared with the impurity formation energy ( $E_{\text{Imp}}^{\text{OB}}$ ) in bulk Si, calculated as

$$E_{\text{Imp}}^{\text{OB}} = E_{n_{\text{OB}}} - E_{\text{B}} - n_{\text{O}}\mu_{\text{O}} \quad (2)$$

$E_{n_{\text{OB}}}$  and  $E_{\text{B}}$  are the total energies of Si bulk containing  $n_{\text{O}}$  number of O atoms and of pristine Si bulk, respectively.

Applying GS and LS methodologies to the LE  $\Sigma 3\{111\}$  Si-GB, we constructed a series of strained structures, which differ by the percentage of strain, for which we calculated the impurity formation energy as

$$E_{\text{Imp}}^{\text{SOGB}} = E_{n_{\text{OSGB}}} - E_{\text{GB}} - n_{\text{O}}\mu_{\text{O}} \quad (3)$$

where  $E_{n_{\text{OSGB}}}$  is the total energy of the strained GB including  $n_{\text{O}}$  number of O atoms.

To keep the effect of the strain during the simulation, it is important not to fully relax the strained structures, which would

prefer to relax to their unstrained counterpart.<sup>[26]</sup> Therefore, comparing the energy from a self-consistent calculation and the optimized structure with imposing constrains around the O atom to preserve the distortion as they differ by about  $3 \times 10^{-3}$  eV, we resort to the self-consistent calculation.<sup>[19]</sup>

In **Figure 2**, we show the formation energies with different numbers of interstitial O ( $n = 1, 2, 3$ , and 4). In Si bulk (Figure 2a) and Si-GB (Figure 2b), energies are almost of similar order. With increasing number of O atoms, the lowering of formation energy suggests more stable and hence more favorable systems. This trend is preserved in the presence of applied strain. Moreover, for GS (Figure 2c), compression is much more effective than elongation in destabilizing the system; actually, with GS  $-3.0\%$ , the formation energy becomes positive and only an increasing number of O atoms is able to stabilize the GB. If the system better sustains a global tensile strain with a large number of O atoms, it is probably a consequence of the fact that Si and O can mimic the  $\text{SiO}_2$  configuration, where the lattice parameter is larger with respect to Si. In case of LS (Figure 2d), several varieties have been adopted, like different percentages of tensile or compressive strains at both sides of O atoms or a mixed strain, with elongation at one side and compression of the same order of magnitude on the other side ( $p = \pm 5.7\%$ ,  $\pm 15.0\%$ , and  $\pm 30.0\%$ ). Figure 2d suggests that the system is really stable for LS up to  $\pm 15.0\%$  for different number of interstitial O, and only a very large LS (30%) with a small number of O atoms induces a positive formation energy.

We then considered how the electronic properties change as a function of strain by focusing only on the systems with  $n = 1$  and  $n = 4$  O atoms; actually, we have observed that with  $n = 2$

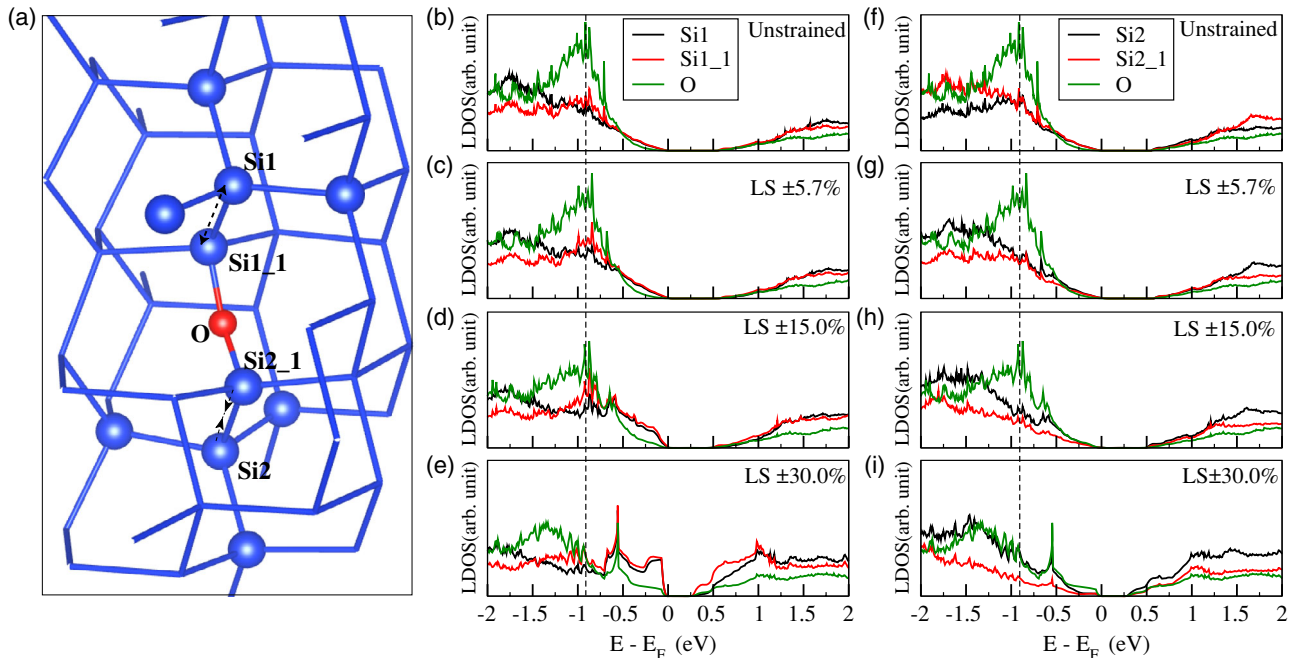


**Figure 4.** a) LS structure with one O. Si1 and Si2 are the two sites with reference of which strain has been generated and Si1\_1, Si2\_1 marked the nearest neighbor site. Black dashed arrows refer to compressed ( $- \rightarrow - < -$ ) or elongated ( $< - - >$ ) bonds. LDOS: Left panel b–e) Si1, Si1\_1, O and right panel f–i) Si2, Si2\_1, O for unstrained and different LS scenarios, as mentioned in the inset.

**Table 1.** Bandgap (eV) for Si-GBs with only interstitial and along with global and LS for ( $n = 1$  and  $n = 4$ ) oxygen atoms.

Configurations	1O	4O
Interstitial	0.551	0.557
GS + 3.0%	0.552	0.545
GS + 0.5%	0.553	0.557
GS - 0.5%	0.548	0.557
GS + 3.0%	0.508	0.541
LS + 5.7%	0.533	0.557
LS + 5.7%	0.544	0.548
LS + 5.7%	0.543	0.550
LS + 15.0%	0.474	0.527
LS + 30.0%	0.283	0.362

and  $n = 3$ , O atom systems follow a similar trend like formation energy variation.

In **Figure 3a**, we plotted the local density of states (LDOS) for the unstrained GB with 1O (left), strained GB with global tensile strain, GS + 3.0% (center), and global compressive strain, GS - 3.0% (right). Through this comparison, it was then possible to clearly analyze how the electronic properties change because of strain. To plot the LDOS, we have chosen Si atoms first neighbors of the O and a Si atom (Si<sub>GB</sub>) far from the GB region of the pristine GB cell. Comparing the unstrained LDOS with the tensile GS of +3.0% and the compressive GS of -3.0%, we observe that there is no particular modification on band edge states or the presence of new gap states.

However, due to the elongation (compression) of the Si–O bonds, the delocalization (localization) of the charge density enhances (reduces) the LDOS peak intensity for 1O atom.

In **Figure 3b**, we repeated the same analysis but for the GB with 4O atoms. We obtained the same behavior as for 1O case, although changes are weaker with respect to the unstrained structure. This is consistent with the lowering of the impurity formation energy for the 4O with respect to the 1O atom. Both for 1O and 4O atoms, comparing LDOS of Si around O with that of Si<sub>GB</sub>, we observe that the formation of Si–O bonds introduces new peaks for both Si and O atoms in the energy region of around -1.0 eV for 1O and -1.25 eV for 4O. Moreover, in both sets of figures, the effect of strain on the shift of these new peaks actually (as shown by black arrows) is clear; while tensile strain shifts peaks higher in energy, nearer to the top of the valence band, compressive strain pushes states to lower energies, deeper in the valence band, with respect to unstrained structures.

In **Figure 4**, we show an example of strained Si-GB with 1O (a) and the LDOS (b–i) of the Si atoms and of the O atom, as indicated in (a) in the case of an applied LS. The applied strain along Si1–Si1<sub>1</sub> and Si2–Si2<sub>1</sub> bonds resorts to a deformation of bond length between other three nearest neighboring sites of Si1 and Si2, as shown with balls in **Figure 4a**. In each considered structure, we have a mixed strain (LS ± 5.7%, LS ± 15.0%, and LS ± 30.0%), which means that we have elongation along Si1–Si1<sub>1</sub> and compression along Si2–Si2<sub>1</sub>. Therefore, **Figure 4b–e** shows mainly the effect of tensile strain, while **Figure 4f–i** shows mainly the effect of compressive strain. In both cases, it is clear that the electronic properties of this GB are really robust: the smaller distortion (±5.7%) has a negligible effect on LDOS and only a strain around or above ±15.0% is able to alter the electronic configuration of the systems, by

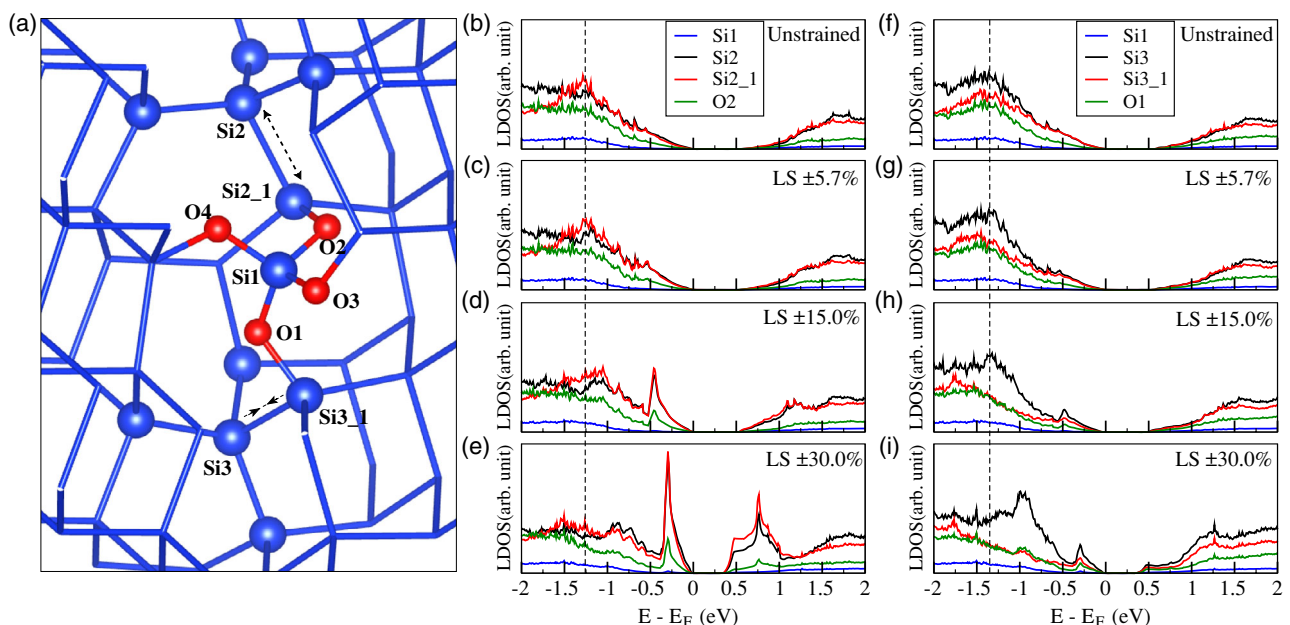


**Figure 5.** a) LS structures with four O and Si2 and Si3 are the two sites with reference of which strain has been generated and Si2<sub>1</sub>, Si3<sub>1</sub> marked the nearest neighbor sites; black dashed arrows refer to compressed (—>—<—) or elongated (<— —>) bonds. LDOS: left panel b–e) Si1, Si2, Si2<sub>1</sub> and O2 and right panel f–i) Si1, Si3, Si3<sub>1</sub>, O1 for unstrained and different LS scenarios, as mentioned in the inset.

changing the peak intensity as well as the energy gap (Table 1). We would like to note that the +15.0% tensile strain is a sort of borderline configuration in which the Si1–Si1<sub>1</sub> are very weakly bonded (2.687 Å). This causes the presence of new structures in the LDOS for Si1 and Si1<sub>1</sub> at the valence band edge that tend to become defect states. This behavior is enhanced when a +30.0% strain is introduced, as shown in (e). In this case also new conduction band edge states are visible. Compression shown in (g–i) seems to reproduce the same trend but is much less effective because the tetrahedral configuration is preserved and no dangling bonds are formed.

For Si-GB with 4O, the LDOS of O1 and O2 and the nearest-neighbor Si atoms, that is, Si1, Si2, Si2<sub>1</sub>, and Si1, Si3, Si3<sub>1</sub>, are shown in Figure 5. Here, the impact of strain is consistent with 1O; moreover, changes in the valence and the conduction band edges, for medium ( $\pm 15.0\%$ ) and large ( $\pm 30.0\%$ ) strain, show clearly the presence of defect states due to the formation of dangling bond as a consequence of strong distortions. This is mostly evident in Figure 5e with high spikes around  $-0.25$  and  $+0.75$  eV, where the tensile strain is applied between Si2 and Si2<sub>1</sub>.

Bandgap values of both GS and LS structures are reported in Table 1. We can observe that bandgap changes are more significant in the GB with 1O atom only, where compressive GS redshift the gap, while tensile strain is essentially ineffective. In the presence of 4O atoms, the system is instead really stable. Actually the relative variation of the bandgap from unstrained structure is maximum,  $\approx 5 \times 10^{-2}$  (eV), for interstitial O atoms ( $n = 1$  and  $n = 4$ ), when the strain is less than 15.0% both global or local. Only above this limit, LS starts to have a significant impact on the electronic gap. In principle, specifically for this indeed stable Si-GB and with interstitial O impurities, vacancy defect would lead to such a high local distortion or coordination defects, as required, to modify the electronic properties<sup>[19]</sup> significantly.

Moreover, considering that, as previously discussed, LS imposes a more inhomogeneous strain field compared with GS, we have analyzed the charge redistribution through the calculation of the charge density difference (CDD), that is, the difference between the charge density of the strained system with respect to the unstrained one. In Figure 6a–d, CDD has been plotted for 1O with LS + 5.7%, LS  $\pm$  5.7%, LS  $\pm$  15.0%, and LS  $\pm$  30.0%. As this plot is of similar nature for 4O atoms, we have discussed here only the case with 1O atom. In Figure 6, CDD is locally concentrated on the strained bonds, as expected. In particular, in Figure 6a,b, CDD for LS + 5.7% and LS  $\pm$  5.7% are shown to compare tensile-only and mixed-strain scenarios, whereas the effect of different amplitudes of LS can be observed from Figure 6b–d. Considering that cyan isosurfaces correspond to lower charge density while yellow ones correspond to higher charge density, with respect to the unstrained system, it is evident that the elongation (compression), shown with dashed arrows in the figure, leads to less (more) charge localization on the strained bonds. Actually, for mixed strain (Figure 6b–d), the yellow isosurface of CDD in the lower part of the structure, where the bond is compressed, and the cyan one in the upper part, where the bond is elongated (similar to the LS + 5.7% configuration (Figure 6a)), clearly show the different nature and different effect of the applied LS. Increasing the percentage of applied tensile and compressive LS (Figure 6b–d) along Si–Si bonds, the

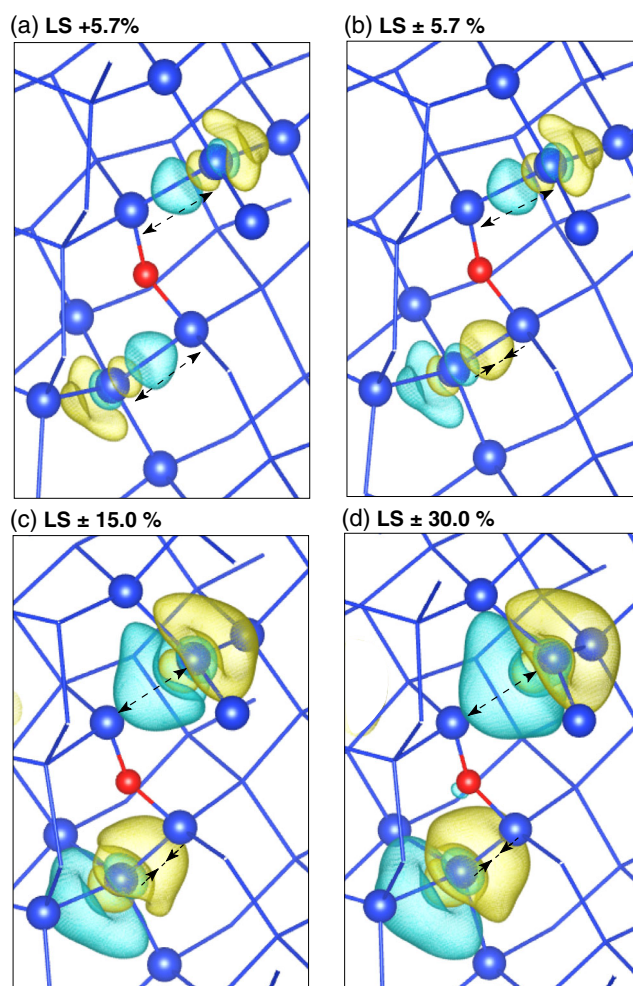


**Figure 6.** Difference of charge density with respect to unstrained structure for 1O with a) LS + 5.7%, b) LS  $\pm$  5.7%, c) LS  $\pm$  15.0%, and d) LS  $\pm$  30.0%. Yellow (cyan) color corresponds to isosurface value:  $+0.007(-0.007)$ . Yellow (cyan) color indicates more (less) amount of charge localization with respect to the unstrained structure. Black dashed arrows refer to compressed ( $- > - < -$ ) or elongated ( $< - - >$ ) bonds.

delocalization and localization of charge density, respectively, become more pronounced.

Finally, to understand the evolution of the bonding structure under LS, we have analyzed the behavior of the electron localization function (ELF).<sup>[27]</sup> In Figure 7, ELF profile is plotted across the strained region, and the distorted (elongated/compressed) Si–Si bonds in our study, are shown for 1O (Figure 7a,b) and 4O (Figure 7c,d) configurations, considering unstrained and mixed-LS scenarios. ELF is a relative measurement of the electron localization and it takes values in the range between 0 and 1. We note that in the PAW method only valence electrons are taken into account in the calculation and for this reason we have the zero value in the ELF profile in the core of the atoms. When the amplitude of ELF is  $\approx 1$ , then electrons are localized in the bonding regions, as observed for unstrained configurations (black line), preserving the symmetric linear profile of the homopolar Si–Si bond. The same symmetric ELF profile can be observed in the case

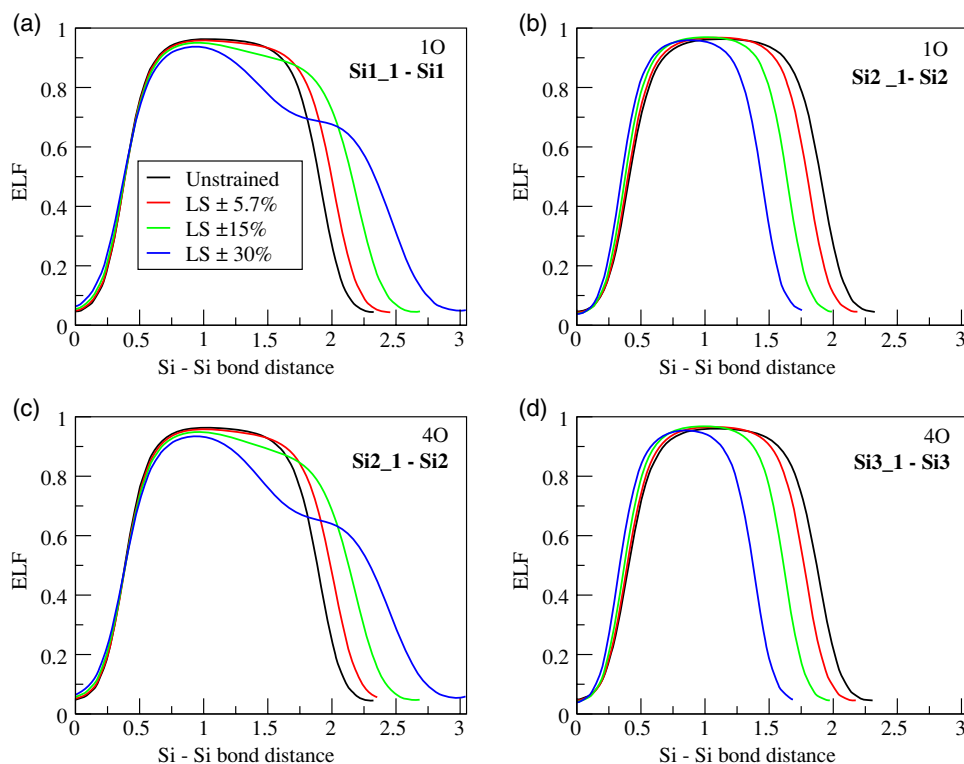


**Figure 7.** ELF profile across the Si–Si strained bond, as indicated by the black dashed arrows in Figure 4a and 5a, for mixed-strain configuration with 1O: a) elongated bond Si1–Si1<sub>1</sub>, b) compressed bond Si2–Si2<sub>1</sub>, and with 4O: c) elongated bond Si2–Si2<sub>1</sub>, d) compressed bond Si3–Si3<sub>1</sub>, respectively.

of compressive strain (Figure 7b,d), where the tetrahedral coordination is preserved and the reduction of the Si–Si bond length results in a stronger electron localization. Concerning the tensile strain, Figure 7a,c shows a different ELF profile that progressively loses its symmetry with increasing percentage of strain. Actually, for strong elongation, the bond begins to dissolve and for the maximum LS of  $\pm 30.0\%$ , the electron, no more involved in a bond, tends to localize more toward one Si atom (Si1<sub>1</sub> for 1O and Si2<sub>1</sub> for 4O) than the other (Si1 for 1O and Si2 for 4O). The ELF analysis confirms and clarifies the effect of different strain categories applied to the considered GBs on the local charge redistribution.

#### 4. Conclusion

In conclusion, formation energy depends on geometrical distortions, either distributed homogeneously or inhomogeneously under the GS or LS model and on the number of impurity precipitates. We observe that the electronic properties are almost unchanged in the presence of a small strain and formation energies decrease with increasing number of O atoms. For GS, this can be explained by the fact that silicon atoms preserve their tetrahedral coordination. Moreover, global tensile strain resulted to be relatively preferable for the GB stability due to the fact that under tensile strain, silicon and oxygen can mimic the structure of SiO<sub>2</sub>, which in fact has a larger lattice parameter than Si. Considering instead the effect of local distortion (Figure 4 and 5) while small strain is essentially ineffective, strong tension above +15%, as the one eventually produced

by vacancies, is more efficient than compression in changing the electronic properties of the GBs. Actually a large tension can induce dangling bonds formation and the presence of defect states in the gap. Moreover, through the analysis of the charge density and of the ELF, we have demonstrated that while the bond elongation reduces the charge density localized on the bond, the compression increases it. The fact that a strain below 15.0% does not directly affect the electrical activity of this particular Si-GB, thus even with oxygen precipitates, preserving the robustness of electronic properties could be a useful information in modeling devices with such samples. However, the electronic properties and the effect of interstitial oxygen(s) and applied strain may vary with different types of Si-GB geometries and this needs to be analyzed in more detail.

#### Acknowledgements

The authors would like to thank the University of Modena and Reggio Emilia for the financial support (FAR dipartimentale 2020) and Centro Interdipartimentale En&Tech, as well as the CINECA HPC facility, for the approved ISCR C project SiGB-NMI (Isc86\_SiGB-NMI).

Open Access Funding provided by Università degli Studi di Modena e Reggio Emilia within the CRUI-CARE Agreement.

#### Conflict of Interest

The authors declare no conflict of interest.

## Data Availability Statement

Research data are not shared.

## Keywords

first principles, oxygen impurities, silicon grain boundaries, strain

Received: July 29, 2021

Revised: November 10, 2021

Published online:

- 
- [1] M. A. Green *Prog. Photovolt.: Res. Appl.* **2009**, *17*, 183.
- [2] L. Chen, X. Yu, P. Chen, P. Wang, X. Gu, J. Lu, D. Yang, *Sol. Energy Mater. Sol. Cells* **2011**, *95*, 3148.
- [3] M. A. Green, K. Emery, Y. Hishikawa, W. Warta, E. D. Dunlop, D. H. Levi, A. W. Y. Ho-Baillie, *Prog. Photovolt.: Res. Appl.* **2017**, *25*, 3.
- [4] M. Hermle, F. Feldmann, M. Bivour, J. C. Goldschmidt, S. W. Glunz, *Appl. Phys. Rev.* **2020**, *7*, 021305.
- [5] R. Maji, J. Contreras-García, N. Capron, E. Degoli, E. Luppi, *J. Chem. Phys.* **2021**, *155*, 174704.
- [6] P. Käshammer, T. Sinno, *J. Appl. Phys.* **2013**, *114*, 083505.
- [7] V. Yu. Lazebnykh, A. S. Mysovsky, *J. Appl. Phys.* **2015**, *118*, 135704.
- [8] Y. Ohno, K. Kutsukake, M. Deura, I. Yonenaga, Y. S. Ebisawa, K. Inoue, Y. Nagai, H. Yoshida, S. Takeda, *Appl. Phys. Lett.* **2016**, *109*, 142105.
- [9] M. Fukuzawa, M. Yamada, *Mater. Sci. Semicond. Process.* **2006**, *9*, 266.
- [10] M. Becker, H. Scheel, S. Christiansen, H. P. Strunk, *J. Appl. Phys.* **2007**, *101*, 063531.
- [11] S. He, S. Danyluk, I. Tarasov, S. Ostapenko, *Appl. Phys. Lett.* **2006**, *89*, 111909.
- [12] J. Chen, B. Chen, T. Sekiguchi, M. Fukuzawa, M. Yamada, *Appl. Phys. Lett.* **2008**, *93*, 112105.
- [13] M. Nacke, M. Allardt, P. Chekhonin, E. Hieckmann, W. Skrotzki, J. Weber, *J. Appl. Phys.* **2014**, *115*, 163511.
- [14] V. Pogue, S. N. Melkote, B. Rounsaville, S. Danyluk, *J. Appl. Phys.* **2017**, *121*, 085701.
- [15] P. Gundel, M. C. Schubert, F. D. Heinz, W. Kwapil, W. Warta, G. Martinez-Criado, M. Reiche, E. R. Weber, *J. Appl. Phys.* **2010**, *108*, 103707.
- [16] G. Sarau, S. Christiansen, M. Holla, W. Seifert, *Sol. Energy Mater. Sol. Cells* **2011**, *95*, 2264.
- [17] Y. Ohno, K. Inoue, K. Fujiwara, M. Deura, K. Kutsukake, I. Yonenaga, Y. Shimizu, K. Inoue, N. Ebisawa, Y. Nagai, *Appl. Phys. Lett.* **2015**, *106*, 251603.
- [18] Y. Ohno, K. Inoue, K. Fujiwara, K. Kutsukake, M. Deura, I. Yonenaga, N. Ebisawa, Y. Shimizu, K. Inoue, Y. Nagai, H. Yoshida, S. Takeda, S. Tanaka, M. Kohyama, *Appl. Phys. Lett.* **2017**, *110*, 062105.
- [19] R. Maji, E. Luppi, N. Capron, E. Degoli, *Acta Mater.* **2021**, *204*, 116477.
- [20] G. Kresse, J. Hafner, *Phys. Rev. B* **1993**, *47*, 558.
- [21] G. Kresse, J. Furthmüller, *Phys. Rev. B* **1996**, *54*, 11169.
- [22] H. J. Monkhorst, J. D. Pack, *Phys. Rev. B* **1976**, *13*, 5188.
- [23] P. E. Blöchl, O. Jepsen, O. K. Andersen, *Phys. Rev. B* **1994**, *49*, 16223.
- [24] K. Momma, F. Izumi, *J. Appl. Crystallogr.* **2011**, *44*, 1272.
- [25] Y. Ohno, K. Inoue, K. Fujiwara, K. Kutsukake, M. Deura, I. Yonenaga, N. Ebisawa, Y. Shimizu, K. Inoue, Y. Nagai, H. Yoshida, S. Takeda, S. Tanaka, M. Kohyama, *J. Microsc.* **2017**, *268*, 3.
- [26] E. Luppi, E. Degoli, M. Bertocchi, S. Ossicini, V. Vénier, *Phys. Rev. B* **2015**, *92*, 075204.
- [27] B. Silvi, A. Savin, *Nature* **1994**, *371*, 683.